

Semi-Siamese Network for Robust Change Detection Across Different Domains with Applications to 3D Printing

Yushuo Niu¹, Ethan Chadwick², Anson W. K. Ma², and Qian Yang¹

¹ Computer Science and Engineering Department, University of Connecticut, Storrs, USA

² Chemical and Biomolecular Engineering Department, University of Connecticut, Storrs, USA

Abstract. Automatic defect detection for 3D printing processes, which shares many characteristics with change detection problems, is a vital step for quality control of 3D printed products. However, there are some critical challenges in the current state of practice. First, existing methods for computer vision-based process monitoring typically work well only under specific camera viewpoints and lighting situations, requiring expensive pre-processing, alignment, and camera setups. Second, many defect detection techniques are specific to pre-defined defect patterns and/or print schematics. In this work, we approach the automatic defect detection problem differently using a novel Semi-Siamese deep learning model that directly compares a reference schematic of the desired print and a camera image of the achieved print. The model then solves an image segmentation problem, identifying the locations of defects with respect to the reference frame. Unlike most change detection problems, our model is specially developed to handle images coming from different domains and is robust against perturbations in the imaging setup such as camera angle and illumination. Defect localization predictions were made in 2.75 seconds per layer using a standard MacBookPro, which is comparable to the typical tens of seconds or less for printing a single layer on an inkjet-based 3D printer, while achieving an F1-score of more than 0.9.

Keywords: change detection · defect localization · semi-siamese neural network · domain adaptation · 3D printing

1 Introduction

Defect detection methods that can provide feedback in real-time is of significant interest to the additive manufacturing community in order to save on materials cost, printing time, and most importantly, to ensure the quality of printed parts. A key advantage of 3D printing technology that can be leveraged to enable *in situ* defect detection is that objects are printed layer by layer (Figure 1). Thus, each 2D layer of the object can be imaged and probed for internal defects; unlike

traditional manufacturing processes, it is not necessary to wait to analyze the fully printed 3D object.

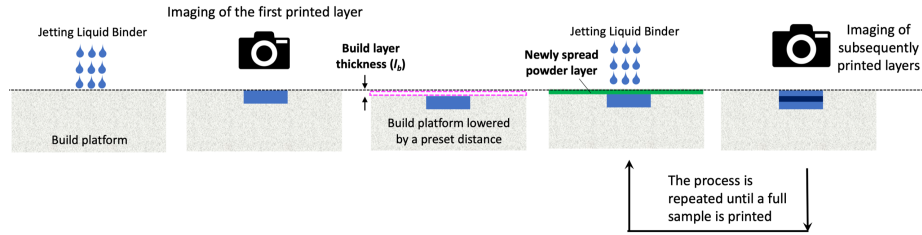


Fig. 1. Schematic diagram of the 3D printing process for binder jet 3D printing with layer-wise imaging during the print.

In this work, we propose a novel defect detection method for 3D printing that poses the problem as one of change detection between a desired reference schematic and a camera image of the printed layer (Figure 2). In the change detection problem in computer vision, two images such as satellite images of land or surveillance images of streets are compared for differences. There are several challenges common to both the defect detection and change detection problems: the need to pre-process and pre-align images due to changes in camera angle and lighting, which result in significant and sometimes expensive limitations to the camera setup that must be used, and the data-hungry nature of this complex comparison problem. Additionally, there are challenges unique to defect detection for 3D printing that are rarely addressed in the change detection literature. In particular, the images we would ideally like to compare for 3D printing are not two camera images, which are from the same image domain, but rather a reference print schematic and a camera image of the actual printed result, which arise from very different image domains. In this work, we utilize one-shot learning techniques [13] to develop a novel deep learning architecture that can provide fast detection of defects robust to camera angle and lighting perturbations. A key innovation of our model is that it enables direct comparison of images arising from different domains. The simplicity and flexibility of our model will enable it to be highly transferable to different industrial settings for 3D printing, without requiring careful camera setups and application-specific model customization that is both expensive and time-consuming. Our proposed approach of building on change detection methods from computer vision for tackling the challenges of defect detection is to the best of our knowledge a new direction in the 3D printing field.

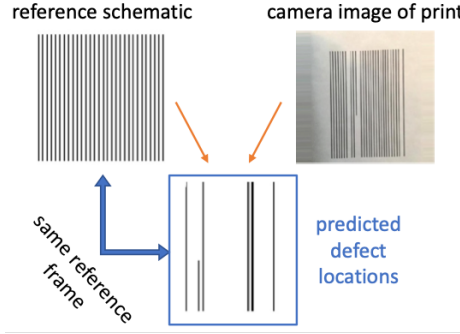


Fig. 2. Our robust defect localization model takes as input a reference print schematic and a camera image of the print, and predicts the precise location of defects with respect to the frame of reference of the print schematic. This model requires 2.75 seconds for prediction, while printing a single layer on an inkjet-based 3D printer requires tens of seconds or less.

2 Related work

Change detection is a fundamental task in computer vision, with many important applications such as analysis of satellite imagery for agricultural monitoring [11], urban planning [17], and disaster assessment [21], among others. A large body of work has thus been built starting from at least the 1980s using methods such as change vector analysis [14]. To handle perturbations such as misalignment and varied lighting, techniques such as incorporating active camera relocation have been proposed [5]. Many state-of-the-art methods today are now based on deep learning, ranging from autoencoders to Siamese neural networks to recurrent neural networks, and various combinations thereof [20]. Recently, several methods based on combining convolutional neural networks (CNN) with Siamese architectures have been proposed. One of the earlier such methods, ChangeNet, uses a combination of ResNet, fully connected, and deconvolution blocks in its Siamese branches [22]. It is designed to handle different lighting and seasonal conditions in the images, but like most existing methods assumes aligned or nearly aligned image pairs. Interestingly, the architecture is different from traditional Siamese architectures in that the deconvolution layers are not required to have the same weights. This is reminiscent of our proposed semi-Siamese architecture which we will discuss in Section 3; however, we will propose the opposite - the deconvolution layers are the portion of our architecture that are required to share the same weights. Another interesting recent approach uses a Siamese pair of autoencoders [15], where the change map is generated based on the learned latent representations. However, this method also assumes coregistered images and can only learn approximate change locations in addition to a classification of whether changes have occurred. A recently proposed architecture that enables fast pixel-level change detection is FC-Siam-diff, a fully convolutional encoder-decoder network with skip connections [3]. In this model, there

are two encoders that share the same architecture and weights, while there is only one decoder. However, this model again assumes coregistered images. Finally, the challenge of dealing with images that are not necessarily coregistered, with differences in lighting, camera viewpoint, and zoom, was recently addressed in Sakurada & Okatani [18] and with CosimNet [6]. The former uses features learned from CNNs trained for large-scale object recognition in combination with superpixel segmentation to address the problem of change detection in pairs of vehicular, omnidirectional images such as those from Google Street View. The latter, CosimNet, uses the DeeplabV2 model as a backbone and proposes various modifications to the loss function to provide robustness to perturbations [6]. Nevertheless, both of these methods still assume that the images being compared are from the same domain, e.g. they are both camera or satellite images, rather than from different domains such as a camera image versus a schematic.

Despite its importance for additive manufacturing, defect detection has traditionally been a challenging task. First, there are many different types of defects that may be of interest, including defects caused by missing jets, inconsistent jets, angled jets, and cracks in powder bed material, just to name a few that are relevant to inkjet-based 3D printing; other technologies such as fused deposition modeling have their own set of defects. Many heuristic-based methods such as computing the entropy of depth maps have consequently been developed to address specific defect types [4]. In recent years, both classical machine learning methods such as support vector machines utilizing human-engineered features [9] and deep learning-based methods utilizing convolutional neural networks have started to be developed to enable more powerful defect detection [10,19]. However, many of these methods require large amounts of labeled experimental data, which is difficult to obtain. They also typically require fixed, high-resolution camera setups, and cannot easily handle differences in camera angle and lighting. For example, one group of methods is based on denoising autoencoders [8], where the idea is that an autoencoder is trained to take as input a “noisy” (defective) image and output its non-defective counterpart. Then, differences between the input and output can be used to identify defects. An advantage of this approach is that it does not require a large amount of labeled experimental data; however, unlike change detection approaches which can handle general differences, this approach can only handle a pre-defined range of defects, since it must be trained to be able to remove them from the output.

3 Semi-Siamese defect detection model

Our proposed model consists of two major components: a novel semi-Siamese architecture based on U-Net [16] branches, and a fully convolutional network (FCN) to reconstruct the final defect detection mask. A diagram of our method is shown in Figure 3, *upper*. The input to the model is a pair of 2D images corresponding to a particular layer during 3D printing: the reference schematic images of the desired print pattern, $I_{ref} \in R^{H \times W \times 3}$, and the camera images of the printed result, $I_{cam} \in R^{H \times W \times 3}$. The image pair (I_{ref}, I_{cam}) is first fed

into a semi-Siamese network to generate a pair of feature maps (F_{ref}, F_{cam}) of the same dimensions as the input. In contrast to standard Siamese networks and existing semi-Siamese networks which use different decoders, a simple but key innovation of our architecture is that the feature extraction sections of each branch (encoder) do not share the same weights; only the reconstruction section (decoder) share the same weights. This is important for our defect detection problem, since the camera image and reference schematic come from different domains. Thus in order to compare them, we would first need to use *different* feature extraction functions to transform them both to the same latent feature space, after which we can then reconstruct them both in a comparable reference frame using the *same* reconstruction function. Then, the Euclidean distance is used to calculate the change map. It is important to calculate the change map from the reconstructed images in a comparable reference frame rather than from the latent feature space in order to enable highly precise pixelwise defect localization. The final FCN is then used to fully transform the change map from this comparable reference frame back to the reference frame of the schematic image.

3.1 Transfer learning from U-Net models

As described above, the semi-Siamese branches of our model are based on the U-Net architecture. This choice is made to leverage the ability of U-nets to produce high resolution outputs [16], enabling precise localization of defects upon comparison of the outputs (F_{ref}, F_{cam}) from each branch. In order to further improve the performance of our model, we first utilize transfer learning from a U-Net model with the same architecture as our semi-Siamese branches (Figure 3, *lower*). This U-net model takes as input a perturbed camera image, and outputs a transformation of the image into the same reference frame as its corresponding reference print schematic. When trained on a fixed number of reference schematics, this U-Net can be used for detecting defects by directly comparing a camera image transformed into the reference frame with its corresponding print schematic. However, it is important to note that this architecture cannot handle arbitrary print schematics. Suppose that we would like to detect defects in a print corresponding to a schematic (called “schematic-new”) that is similar to a print schematic that the model was previously trained on (called “schematic-old”), but looks like a perturbed version of that schematic. Then any camera images of a perfect print of “schematic-new” might be erroneously transformed by the model back into the reference frame of “schematic-old”. Now when compared with “schematic-new”, many defects will be detected, even though no defects occurred in the actual print. Thus, this U-Net architecture cannot be used on its own to handle defect detection for arbitrary desired print schematics. We will instead use this U-Net model pre-trained on a small set of reference schematics to initialize the weights of each branch of our semi-Siamese model. This allows us to initialize the semi-Siamese model in such a way that it can offset perturbations for some limited set of camera images and reference schematics. We

then continue training to fine-tune these weights to be able to handle arbitrary reference print schematics and perturbed camera images.

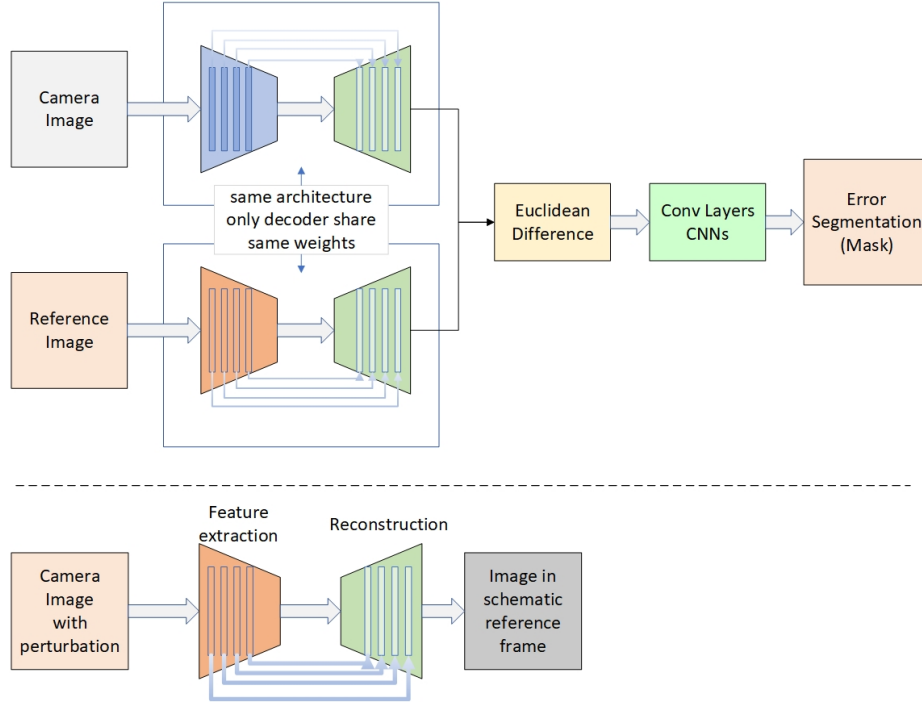


Fig. 3. (upper) Schematic of our proposed semi-Siamese model. The two branches share the same architecture, however only the reconstruction blocks (green trapezoids) share the same weights. (lower) Schematic of the U-Net model that we use for transfer learning. The orange trapezoid represents the feature extraction blocks, while the green trapezoid represents the reconstruction blocks. Silver lines are used to represent skip connections.

3.2 Semi-Siamese network architecture

Our deep learning model begins with two U-Net branches sharing an identical architecture. Each U-Net has five fully convolutional blocks to do downsampling (feature extraction) and four convolutional blocks to do upsampling (reconstruction). Each feature extraction block is composed of two 3×3 convolutional layers followed by a rectified linear unit (ReLU) activation. For the first four feature extraction blocks, there is a 2D max pooling layer after each block, where each max pooling layer has pool size 2×2 and strides of 2. For each of the first four feature extraction blocks, the size of the feature maps are thus reduced by half, while the number of channels is doubled. In the last feature extraction block,

there is no max pooling layer, so the size of the feature map remains the same and only the number of channels is doubled. For the reconstruction blocks, each block starts with sub-pixel convolution layers (upsampling layers) followed by 3×3 convolution layers with ReLU activation. Analogous to the feature extraction block, the size is doubled each time but the number of channels is reduced by half. Skip connections link the output from the max pooling layers to the corresponding upsampling layers. From these semi-Siamese branches, a pair of feature maps are generated and their pixel-wise Euclidean distance is calculated to get the change map. This change map is then fed into the remaining FCN, which generates the final change mask \hat{Y} giving the predicted probability that each pixel corresponds to a defect location. Finally, we use a simple threshold on the change mask to derive the pixel-wise defect localization. A full schematic of the proposed architecture is shown in Figure 4.

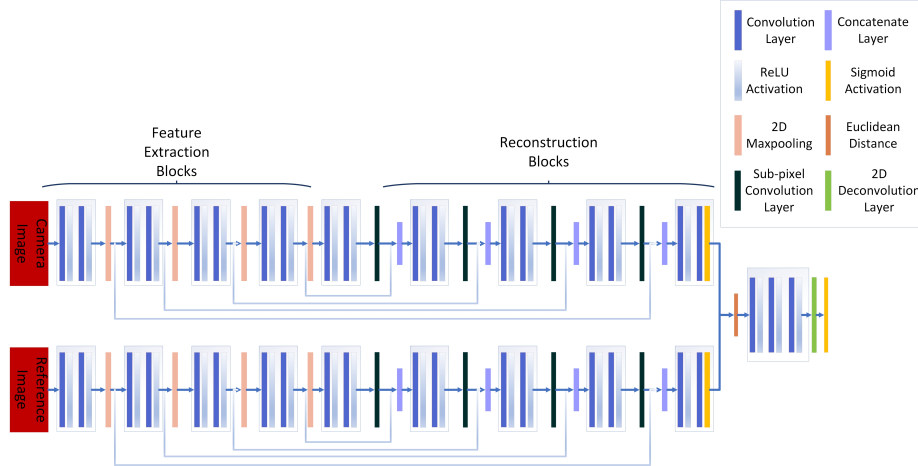


Fig. 4. Full architecture for our model. Different types of layers are labeled by color, as indicated in the legend. The semi-Siamese branches each consist of an underlying U-Net architecture, with a feature extraction (encoder) section, a reconstruction (decoder) section, and skip connections between corresponding layers.

3.3 Training Objective

Our model uses a loss function consisting of two parts: contrastive loss [7] and binary cross-entropy, whose respective contributions are controlled by a hyperparameter λ .

$$L_{all} = L_{bin} + \lambda L_{con} \quad (1)$$

The standard cross-entropy loss for binary classification is applied to the change mask \hat{Y} :

$$L_{bin}(Y, \hat{Y}) = - \sum_{i,j} Y_{ij} \log \hat{Y}_{ij} + (1 - Y_{ij}) \log(1 - \hat{Y}_{ij}) \quad (2)$$

where for a given pixel in the i^{th} pixel row and j^{th} pixel column of the image, $Y_{ij} \in \{0, 1\}$ is the ground truth label and $\hat{Y}_{ij} \in (0, 1)$ is the predicted probability that the pixel corresponds to a location with defects.

The contrastive loss, on the other hand, is applied to the outputs (F_{ref}, F_{cam}) of the semi-Siamese branches. The goal of the contrastive loss is to encourage the semi-Siamese branches to encode locations of no change to similar outputs while enlarging differences in the encodings for the locations where there are true changes/defects. The formulation of the contrastive loss we use is similar to that used by CosimNet [6] and is given by:

$$L_{con}(Y, F_{ref}, F_{cam}) = \sum_{i,j} \begin{cases} D(f_{ij}^r, f_{ij}^c) & , \quad Y_{ij} = 0 \\ \max(0, m - D(f_{ij}^r, f_{ij}^c)) & , \quad Y_{ij} = 1 \end{cases} \quad (3)$$

where $f_{ij}^r, f_{ij}^c \in \mathbb{R}^3$ correspond to the i^{th} row and j^{th} column of F_{ref} and F_{cam} , respectively, and $D(a, b) = \|a - b\|_1$. Here m is a constant called the margin, typically chosen to be 1. Note that when $Y_{ij} = 0$, the model tries to minimize $D(f_{ij}^r, f_{ij}^c)$, while when $Y_{ij} = 1$, the model tries to make $D(f_{ij}^r, f_{ij}^c) > m$ if possible.

4 Experiments

In contrast to typical change detection problems that assume pairs of input images coming from similar domains, our semi-Siamese model is specifically designed for comparing images from different domains: one is a 3D printing reference schematic, while the other is a camera image which may include perturbations to lighting and camera angle. To demonstrate this capability, it is thus unsatisfactory to use existing change detection datasets such as Tsunami [18], GSV [18], and VL-CMU-CD [1], which typically contain pairs of camera images; instead, it is necessary to create our own experimental dataset consisting of images from these two different domains. As a proof of concept, we generated a dataset consisting of pairs of (1) reference print schematics and (2) camera images taken using an iPad Air 2 of those schematics printed on paper using an inkjet printer (Figure 5, *left*). In a true 3D printing experiment, these camera images would correspond to a 2D image of the top layer of a 3D print after each layer is complete. An example of this for inkjet-based 3D printing on powder bed material is shown in Figure 5, *right*. Here Dimatix Blue model fluid is used on Visijet core powder.

To simplify dataset generation, our set of reference schematic images consist only of images with vertical lines of varying length. The corresponding camera

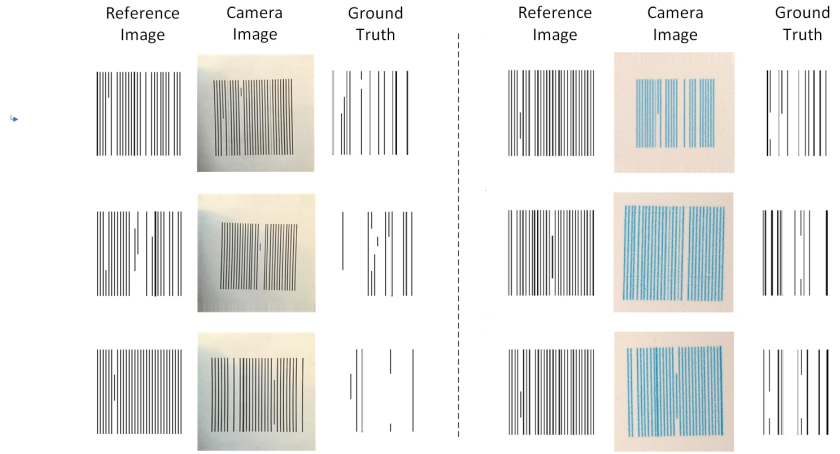


Fig. 5. (left) Examples from our proof-of-concept dataset of schematics printed on paper using an inkjet printer. (right) Examples of similar schematics printed on powder bed material using an inkjet-based 3D printer. Here the “Ground Truth” column corresponds to the true pixelwise locations of defects in the printing results in comparison to the desired “Reference Image”.

images are taken at various angles, so that a simple template matching approach would not be able to easily achieve pixel-wise accuracy in defect localization. In future work, we will expand to more complex schematic images. However, the efficacy of our model can be sufficiently demonstrated using this basic dataset.

4.1 Full dataset generation using data augmentation

Since generating an experimental dataset is time-consuming, and with a real 3D printer also incurs significant material costs, we start with only a limited dataset of 42 pairs of experimental images. We then use data augmentation to significantly increase our dataset size by adding perturbations in camera angle to existing camera images. Note that lighting perturbations come naturally from the camera images being taken using an iPad Air 2 with no special lighting setup. We do not make any changes to the reference schematics. The types of perturbations we use in the data augmentation includes zoom, rotation, shear, and position (width and height) shift. We emphasize that here we use data augmentation to create our initial full dataset, in contrast to the typical setting in computer vision where data augmentation should only be used in training. The perturbations to the camera image given by data augmentation correspond to artificial new “experiments” of different camera setups. To prevent data leakage, we separate the training, validation, and test sets by reference schematic. The final dataset consists of 9,000 training, 900 validation, and 900 test images, where 30 underlying schematic images are used in the training data, and 6 schematic images each were used for validation and test.

To create defective image pairs, we match the camera image from one reference image with a different reference schematic. Since all of the images correspond to perfect non-defective prints for their true corresponding schematic, we can precisely localize the “defects” in the defective image pairs by comparing the camera image’s true reference schematic with the given new schematic. To generate the training, validation, and test sets, we first randomly select either one underlying schematic for non-defective examples, or two different underlying schematics for defective examples. Then we randomly pick corresponding camera images from among the perturbed variations in our augmented dataset. We note that it is important to balance the dataset between defective and non-defective pairs; otherwise the trained model tends to predict the presence of some defects even for non-defective pairs.

We use the class `keras.preprocessing.image.ImageDataGenerator` in Keras [2] for data augmentation. We use zoom range = 0.3, rotation range = 2, shear range = 0.005, width shift range = 0.02, and height shift range = 0.02. See Figure 6 for examples of perturbed images corresponding to the same underlying print schematic.

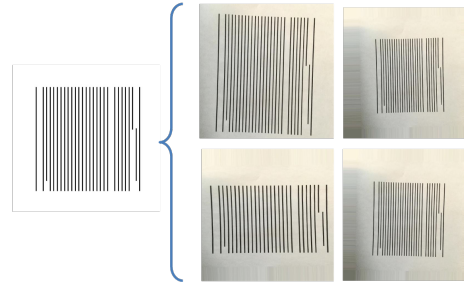


Fig. 6. Examples of perturbations used to create our augmented dataset. While these are larger perturbations in camera angle and lighting than would be typically necessary for an industrial 3D printing setting, the ability of our model to handle these perturbations demonstrates its robustness and potential to reduce the cost of setting up defect detection for new machines.

4.2 Existing algorithms

We compare our model against two existing change detection methods: FC-Siam-diff [3] and CosimNet [6], noting that we do not compare against existing 3D printing defect detection methods because they are not designed to handle different print schematics automatically. While FC-Siam-diff has a more similar encoder-decoder architecture to our proposed method, CosimNet was designed to handle similar types of perturbations to camera angle and lighting as in our application. FC-Siam-diff is a fully convolutional Siamese network for change detection that was designed to be trained end-to-end from scratch without requiring

pre-training. Similarly to our method, it utilizes an encoder-decoder architecture with skip connections to improve spatial accuracy. The FC-Siam-diff model assumes coregistered images, but is able to handle some lighting differences. CosimNet, on the other hand, is designed to handle challenging conditions such as variations in camera angle and lighting. It does not utilize an encoder-decoder architecture. Neither of these models are able to explicitly consider that the images being compared come from different domains, such as a print schematic and a camera image. To make these models suitable for application to our unique experimental dataset, we made a couple of modifications. First, in CosimNet we use our loss function given in (1) instead of the Threshold Contrastive Loss (TCL) proposed in their paper for large camera viewpoint differences, which do not apply to our dataset. Second, instead of using the multilayer side-output training policy described in their model, we only use the top layer of the model as the output layer. Finally, for FC-Siam-diff, we remove all dropout layers to improve performance since our experimental dataset is more challenging than the datasets utilized in their paper. We found empirically that these changes result in better performance on our experimental dataset.

4.3 Implementation details

To train our final semi-Siamese model, as well as the state-of-the-art models FC-Siam-diff [3] and CosimNet [6], we used the following hyperparameters: learning rate: 10^{-5} ; batch size: 4. We use the Adam optimizer [12] with $\beta_1 = 0.9$, $\beta_2 = 0.999$, and $\epsilon = 10^{-8}$. The maximum number of epochs is set to 300, but we use early stopping based on the F1-score, with patience parameter = 30. In the loss function, we use $\lambda = 3$ and $m = 1$ in the contrastive loss. All of our input images have dimensions $480 \times 480 \times 3$ with RGB encoding. We use Keras 2.2.4 with Tensorflow 1.14.0, Python 3.5.2, and Numpy 1.16.3. The hardware we train our models on is one NVIDIA Tesla V100 GPU. Predictions are made on a MacBook Pro with 2.4 GHz Quad-Core Intel Core i5 processor and 16 GB memory.

5 Results

5.1 Evaluation criteria

We report the precision, recall, F1-score, and IoU (intersection over union) of each model. Since our dataset consists of a balanced set of both defective and non-defective image pairs, these metrics are computed with respect to the defect class on defective pairs and with respect to the non-defective class on non-defective pairs, with the final metric being a simple average between the two. We note that since the non-defective class generally corresponds to a larger number of pixels in an image than the defective class, the performance metric values for the non-defective pairs tend to be much higher; that is, prediction mistakes made by the model in the non-defective case tend to correspond to a smaller proportion of the total number of pixels of interest than in the defective case. For this reason, we also report separately the performance on only the defective image pairs.

5.2 Performance results

In Table 1, we provide the performance results of six different models: (1) CosimNet; (2) FC-Siam-diff; (3) using only a U-Net model to undo perturbations before comparing with the reference schematic (U-Net); (4) our proposed architecture without the semi-Siamese component (e.g. keeping the feature extraction/encoder weights the same in both branches) and without transfer learning from a pre-trained U-Net (Siam w/o init); (5) the Siamese architecture with transfer learning added (Siamese); and (6) our final semi-Siamese model that includes transfer learning (Semi-Siam). All experiments were performed on our unique experimental inkjet dataset. Our semi-Siamese model reaches almost or more than 90% accuracy, depending on the performance metric used, which is significantly better than state-of-the-art. Fig. 7 shows example predictions from our model compared to state-of-the-art. We note that our model requires similar training time to state-of-the-art and is able to make predictions in under 3 seconds, which is comparable to the print time per layer in inkjet-based 3D printers.

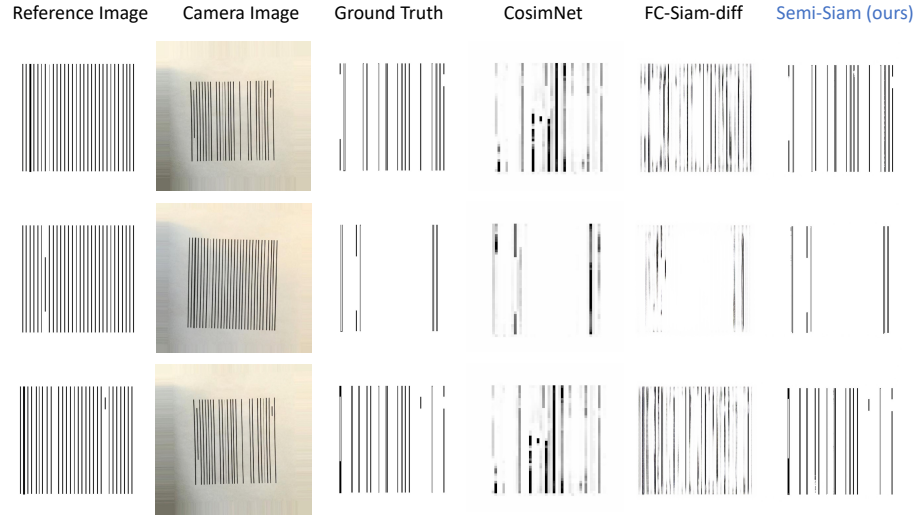


Fig. 7. Examples of predictions from our semi-Siamese model compared to state-of-the-art. Predictions for defects are given in the reference frame of the reference print schematic, enabling precise defect localization regardless of the angle and lighting of the camera image.

5.3 Runtime

In Table 2, we provide the training, model loading, and prediction times of the different model architectures. We note that FC-Siam-diff has the fastest training

Method	Precision	Recall	F1-Score	IoU
CosimNet <i>defect only</i>	0.59	0.54	0.56	0.36
	0.18	0.11	0.13	0.073
FC-Siam-diff <i>defect only</i>	0.81	0.71	0.75	0.65
	0.61	0.43	0.50	0.34
U-Net <i>defect only</i>	0.78	0.77	0.77	0.67
	0.55	0.59	0.56	0.43
Siam w/o init <i>defect only</i>	0.85	0.71	0.76	0.63
	0.70	0.44	0.53	0.37
Siamese <i>defect only</i>	0.94	0.92	0.93	0.87
	0.87	0.84	0.86	0.78
Semi-Siam <i>defect only</i>	0.97	0.95	0.96	0.94
	0.94	0.92	0.93	0.89

Table 1. For each model, the first row of results correspond to the average between defective and non-defective pairs of data, and the second row corresponds to performance on defective pairs only. Our model (Semi-Siamese) performs significantly better than existing state-of-the-art, which were not designed for comparing images from different domains (print schematic versus camera image), and have varying capabilities in handling robustness to perturbations in camera angle and lighting.

time, while CosimNet requires more than twice as long as the other methods for each prediction. Similarly to the simpler FC-Siam-diff and standalone U-Net architectures, our model is able to make predictions in under 3 seconds, which is comparable to the print time per layer in inkjet-based 3D printers.

Method	Train	Load	Prediction
CosimNet	35.98 hr (69 ep)	8.85 s	4.86 s
FC-Siam-diff	6.18 hr (118 ep)	6.82 s	2.76 s
U-Net	24.88 hr (232 ep)	6.75 s	2.40 s
Semi-Siam	34.67 hr (158 ep)	8.18 s	2.75 s

Table 2. After training and initial loading, our model is able to make predictions in 2.75 seconds per pair of schematic and camera images; this is sufficiently fast in comparison to the print time per layer in a typical inkjet 3D printer. Our model takes a comparable amount of training time and has faster loading and prediction time than existing models that handle camera angle and lighting perturbations such as CosimNet. Note the number of epochs used to train are denoted by the abbreviation ep.

5.4 Ablation studies

In this section, we first show that simply using a U-Net model to undo the camera image perturbations before comparison with a reference schematic is insufficient.

The U-Net is only capable of correctly removing perturbations from camera images corresponding to print schematics it has previously been trained on, as explained above in Section 3.1. Table 1 shows that we can improve precision by instead using our proposed architecture even with fully Siamese branches, and that additionally our recall and IoU can be almost doubled by transfer learning from a pre-trained U-Net. Finally, our proposed semi-Siamese model resulted in significantly better performance than all of the above variations, with an improvement of up to 7% for F1 score and 11% for the IOU on defective image pairs in comparison to the purely Siamese model. This shows that the semi-Siamese architecture is critical in enabling superior performance when the images being compared are from different domains.

6 Conclusions

We have developed a new deep learning-based method for change detection where (i) a camera image is being compared against a desired schematic rather than another camera image, and (ii) perturbations to the camera angle and lighting do not need to be pre-corrected, and coregistration is not necessary. This novel semi-Siamese model can be applied to obtain precise *in-situ* pixel-wise defect localization for each layer of a 3D print, enabling rapid detection of internal defects, ensuring the quality of 3D printed parts and saving time and material costs. While an acknowledged limitation of this method is that it does not directly handle defects in the z-direction in a *single* layer, due to the ability to observe each printed layer at various perturbed camera angles, large z-direction defects in the top layer will likely project onto the 2D camera image in such a way as to appear as in-plane defects. Robust handling of these types of defects will be explored in future work.

Defect detection for 3D printing is an important industrial challenge that to the best of our knowledge is being addressed with change detection techniques for the first time in this work. The key benefit of utilizing the change detection framework is that it is not necessary to pre-define the desired print schematic, nor to have a large set of annotated data for each defect type. Our model is capable of detecting defects in a few seconds with more than 90% accuracy. The robustness of our algorithm to camera angle and lighting perturbations, as well as its lower training data requirements, will enable flexibility for utilizing this model in different industrial settings. Furthermore, a capability that has not previously been widely addressed in the computer vision literature is that our model enables a path forward to fast and robust change detection when the input images are from different domains, such as a print schematic and camera image in the 3D printing application discussed here, broadening the types of problems that can be solved with change detection methods.

References

1. Alcantarilla, P., Stent, S., Ros, G., Arroyo, R., Gherardi, R.: Street-view change detection with deconvolutional networks. *Autonomous Robots* **42**, 1301–1322 (2018).

<https://doi.org/10.1007/s10514-018-9734-5>

2. Chollet, F., et al.: Keras. <https://keras.io> (2015)
3. Daudt, R.C., Saux, B.L., Boulch, A.: Fully convolutional siamese networks for change detection. 2018 25th IEEE International Conference on Image Processing (ICIP) pp. 4063–4067 (2018). <https://doi.org/10.1109/icip.2018.8451652>
4. Fastowicz, J., Grudziński, M., Teclaw, M., Okarma, K.: Objective 3d printed surface quality assessment based on entropy of depth maps. *Entropy* **21** (2019). <https://doi.org/10.3390/e21010097>
5. Feng, W., Tian, F., Zhang, Q., Zhang, N., Wan, L., Sun, J.: Fine-grained change detection of misaligned scenes with varied illuminations. 2015 IEEE International Conference on Computer Vision (ICCV) pp. 1260–1268 (2015). <https://doi.org/10.1109/iccv.2015.149>
6. Guo, E., Fu, X., Zhu, J., Deng, M., Liu, Y., Zhu, Q., Li, H.: Learning to measure change: Fully convolutional siamese metric networks for scene change detection. *ArXiv* **abs/1810.09111** (2018)
7. Hadsell, R., Chopra, S., LeCun, Y.: Dimensionality reduction by learning an invariant mapping. 2006 IEEE Computer Society Conference on Computer Vision and Pattern Recognition (CVPR'06) **2**, 1735–1742 (2006). <https://doi.org/10.1109/cvpr.2006.100>
8. joo Han, Y., Yu, H.J.: Fabric defect detection system using stacked convolutional denoising auto-encoders trained with synthetic defect data. *Applied Sciences* **10**, 2511 (2020). <https://doi.org/10.3390/app10072511>
9. Jacobsmühlen, J.Z., Kleszczynski, S., Witt, G., Merhof, D.: Detection of elevated regions in surface images from laser beam melting processes. IECON 2015 - 41st Annual Conference of the IEEE Industrial Electronics Society pp. 001270–001275 (2015). <https://doi.org/10.1109/iecon.2015.7392275>
10. Jin, Z., Zhang, Z., Gu, G.: Autonomous in-situ correction of fused deposition modeling printers using computer vision and deep learning. *Manufacturing letters* **22**, 11–15 (2019). <https://doi.org/10.1016/j.mfglet.2019.09.005>
11. Khan, S.H., He, X., Porikli, F., Bennamoun, M.: Forest change detection in incomplete satellite images with deep neural networks. *IEEE Transactions on Geoscience and Remote Sensing* **55**(9), 5407–5423 (2017). <https://doi.org/10.1109/tgrs.2017.2707528>
12. Kingma, D.P., Ba, J.: Adam: A method for stochastic optimization. *CoRR* **abs/1412.6980** (2015)
13. Koch, G.R.: Siamese neural networks for one-shot image recognition. In: ICML Deep Learning Workshop (2015)
14. Malila, W.A.: Change vector analysis: An approach for detecting forest changes with landsat. In: Proceedings of the 6th Annual Symposium on Machine Processing of Remotely Sensed Data (1980)
15. Mesquita, D.B., Santos, R.F.D., Macharet, D., Campos, M., Nascimento, E.R.: Fully convolutional siamese autoencoder for change detection in uav aerial images. *IEEE Geoscience and Remote Sensing Letters* **17**, 1455–1459 (2020). <https://doi.org/10.1109/lgrs.2019.2945906>
16. Ronneberger, O., P.Fischer, Brox, T.: U-net: Convolutional networks for biomedical image segmentation. In: Medical Image Computing and Computer-Assisted Intervention (MICCAI). LNCS, vol. 9351, pp. 234–241. Springer (2015). https://doi.org/10.1007/978-3-662-54345-0_3
17. Saha, S., Bovolo, F., Bruzzone, L.: Building change detection in vhr sar images via unsupervised deep transcoding. *IEEE Transactions on Geoscience and Remote Sensing* **59**(3), 1917–1929 (2021). <https://doi.org/10.1109/tgrs.2020.3000296>

18. Sakurada, K., Okatani, T.: Change detection from a street image pair using cnn features and superpixel segmentation. In: BMVC (2015). <https://doi.org/10.5244/c.29.61>
19. Scime, L., Siddel, D., Baird, S.T., Paquit, V.: Layer-wise anomaly detection and classification for powder bed additive manufacturing processes: A machine-agnostic algorithm for real-time pixel-wise semantic segmentation. Additive manufacturing **36**, 101453 (2020). <https://doi.org/10.1016/j.addma.2020.101453>
20. Shi, W., Zhang, M., Zhang, R., Chen, S., Zhan, Z.: Change detection based on artificial intelligence: State-of-the-art and challenges. Remote Sensing **12**(10) (2020). <https://doi.org/10.3390/rs12101688>
21. Sublime, J., Kalinicheva, E.: Automatic post-disaster damage mapping using deep-learning techniques for change detection: Case study of the tohoku tsunami. Remote Sensing **11**(9), 1123 (2019). <https://doi.org/10.3390/rs11091123>
22. Varghese, A., Gubbi, J., Ramaswamy, A., Balamuralidhar, P.: Changenet: A deep learning architecture for visual change detection. In: ECCV Workshops (2018). https://doi.org/10.1007/978-3-030-11012-3_10